Selenium chains in ZSM-5 zeolite: Atomic structure and optical properties

A. SAITOH[*], H. TAKEBE, K. TANAKA[a]

Materials and Science and Engineering, Graduate School of Science and Engineering, Ehime University, Matsuyama, 790-8577, Japan
[a]*Department of Applied Physics, Graduate School of Engineering, Hokkaido University, Sapporo, 060-8628, Japan*

Structures and optical properties of selenium-loaded single-crystalline ZSM-5 (z-Se) have been studied. Obtained results are compared with those for bulk Se. Structural measurements using Raman-scattering and X-ray diffraction reveal that Se clusters in the ZSM-5 exist as single chains. Electron-spin resonance (ESR) measurements suggest that the chain has finite lengths of ~5 nm. Optical properties and photoinduced phenomena of z-Se are explored through ESR, absorption (α), and photoluminescence (PL) measurements upon exposure of visible light at room temperature.

1. Introduction

Studies on nano-structured materials attract growing interest [1]. The zeolite, a porous crystal with typical compositions of Al-Si-O having varied structures, has been demonstrated to work as a good matrix for producing well-defined nano-structures. Pioneering work by Bogomolovs' group has demonstrated that a chalcogen behaves as an interesting guest [2-4], partly because the chalcogen forms molecules with ring and chain structures. Substantial (successive and valuable) studies have been published [5-13], which suggest or demonstrate that the chalcogen-loaded zeolite is promising for optical applications. However, as known, there are many (more than a hundred) kinds of zeolites, and studies using covalent zeolite crystals appear to be few.

We here study structural and optical properties of Se-loaded ZSM-5 zeolite (z-Se) with a motivation for new optical devices. The reasons why we select this system are the following: first, we can obtain transparent and sub-mm size ZSM-5 [14-16], which is suitable to single-crystalline, structural, and optical experiments. Second, atomic structures of ZSM-5 are appropriate for Se loading. As schematically illustrated in Fig. 1, it has two kinds of pores [15, 16]; one being parallel to the crystalline *b* axis and the other being zig-zag on the *a-c* plane. Diameters of these pores are approximately the same, with framework and free diameters of ~0.83 nm and ~0.56 nm. Third, ZSM-5 is fairly covalent with the Al/Si ratio of ~ 0.02 [15, 16], so that ionic interaction between loaded Se and pore walls may be the least.

2. Experimental

Preparations of Se-loaded samples are divided in two processes. First, transparent single-crystalline ZSM-5 with a typical dimension of ~$40 \times 40 \times 200$ μm^3 was provided. The ZSM-5 crystals had contained organic templates, which were desorbed by a heat treatment at 500 ºC for 3 h in vacuum just before Se loading. The desorption was confirmed through disappearance of infrared absorption peaks of the template [17]. Second, piles of ZSM-5 and Se chunks with 6N-purity were vacuum-sealed in a double-arms quartz ampoule to two arms separately, which were heated so that the chalcogen was impregnated from vapor phases into the zeolite. The heating condition was selected after several trials, the best being the temperatures of 300 ºC for Se and ~150 ºC for zeolite piles with a treating duration of ~3 h, which could produce dense-colored z-Se samples. The sample was more-or-less stable. At least for 3 years, color change of prepared z-Se was not confirmed under storage in dry atmosphere. However, samples stored for 8 months presented infrared peaks due to H_2O.

Structural and optical properties were inspected. First, an amount of loaded Se was estimated from measurements of weight changes upon thermal desorption of Se. Second, Raman-scattering spectroscopy was performed using a triple-spectrometer system (Jobin Yvon, T64000) equipped with a cooled charge-coupled device. Linearly-polarized Ar$^+$ (wavelengths of 488 and 515 nm) and He-Ne (633 nm) lasers, which provided focused light spots with a diameter of ~1 μm and an intensity of ~50 μW were employed for probe light. Third, X-ray diffraction patterns were obtained using a Cu rotating anode (Rigaku, Ru-300), a conventional diffractometer, and a proportional counter

having a graphite monochromator. Samples, consisting of several hundred z-Se pieces fixed to thin (~30 μm) sheets of highly-oriented pyrolytic graphite, were inspected in a Laue transmission arrangement, which could suppress intense peaks arising from the graphite. Fourth, ESR spectra were monitored using an X-band continuous-wave spectrometer (JEOL, FE1X) at 80 and 290 K. Concentrations of unpaired electrons were estimated by using $CuSO_4 \cdot 5H_2O$ as a standard. Fifth, visible-range transmission spectra were obtained for single samples, which were put on an aperture with a diameter of 25 μm, using a double-beam spectrometer (JASCO, V570) at 80 and 293 K. Sixth, photoinduced absorption under illumination of laser light with photon energies of 2.0-2.6 eV and intensities of 1-40 mW was investigated using a conventional spectrometer. Induced absorption was monitored within ~5 min after interrupting light excitation. Seventh, photoluminescence (PL) was measured using several lasers and the triple-polychromator system at room temperature. Spectral shapes were calibrated using a black-body radiation.

3. Results

Fig. 1 shows color variations of z-Se samples with the corresponding transmission spectra. ZSM-5 is fairly transparent in the visible region, while Fig. 1 shows a small transmittance decrease at short wavelengths, which probably reflects light scattering. Se loading has added color to the zeolite. However, even under the selected condition, z-Se samples produced under a single treatment have appeared in different colors with pale yellow, orange, and brown, the number ratio being roughly 1 : 6 : 3. In addition, single samples possess spatial color variation. These results may imply some imperfections in the present ZSM-5 crystals. Since the brown sample gives the most intense Raman-scattering peak attributable to Se, we focus on the brown in the following.
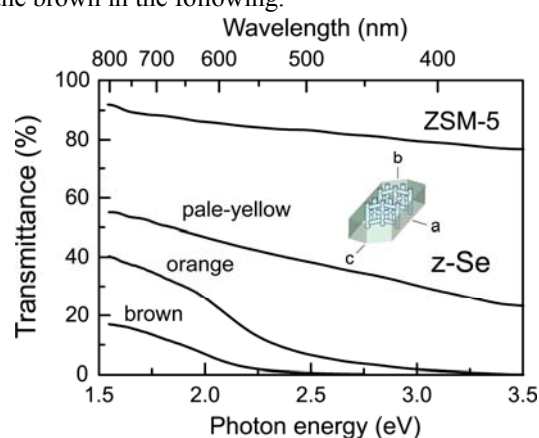

Fig. 1. Transmission spectra of a pure ZSM-5 zeolite (top) and three colored samples. Inset is a schematic illustration of a ZSM-5 crystal, with crystalline axes and exaggerated pores.

Quantities of impregnated Se in a ZSM-5 crystal have been determined through measuring weight loss upon thermal desorption. Measurements were done three times for ~3000 pieces of brown-colored z-Se with total weights of 2.8-3.0 mg, which became transparent with weights of 2.0-2.3 mg after a heat treatment at 250 °C for 20 min. The weight loss of 0.5-1 mg corresponds to ~10^{15} Se atoms per a ZSM-5 crystal. On the other hand, the total length of pores in the ZSM-5 is estimated from the crystal structure [16] at 10^6 m/piece. Accordingly, assuming that the 10^{15} Se atoms take helical chain structures with a helix pitch of ~0.6 nm (see, Table 1), we envisage that ~ 100% pores are filled with Se atoms in brown samples.
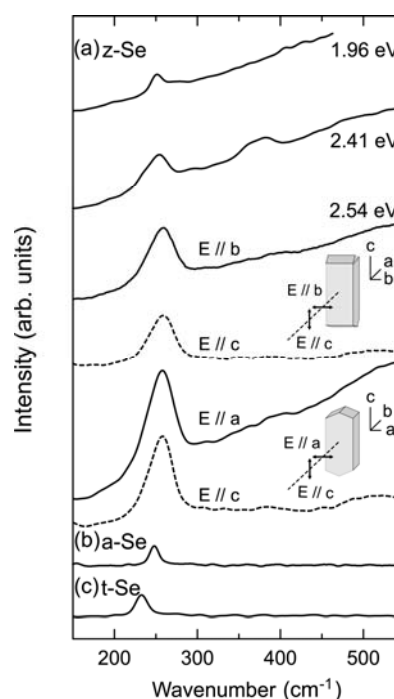

Fig. 2. Raman scattering spectra of (a) z-Se (six traces from the top), (b) a-Se, and (c) t-Se. For z-Se, the top and second spectra are obtained using probe light of 1.96 eV (633 nm) and 2.41 eV (515 nm) with polarization un-resolved. All the others are probed by 2.54 eV (488 nm) light, in which the electric-field E direction and incident plane (a and b) are illustrated in the insets.

Fig. 2 shows Raman-scattering spectra of z-Se, a-Se, and t-Se. The spectra are obtained using linearly-polarized laser light, while the polarization of scattered light is unresolved. We see in Fig. 2 that some peaks appear on flat or oblique baselines. Z-Se inspected under the electric field E of probe light parallel to the zeolite c axis ($E//c$), a-Se, and t-Se shows relatively-sharp Raman-scattering peaks with flat baselines. On the other hand, in all z-Se with E not parallel to the c axis, the baselines increase with the scattering wavenumber, which is attributable to photoluminescence. The main Raman peak is located at ~240 nm^{-1} in t-Se, ~250 cm^{-1} in a-Se, the both being consistent with previous results [18], and ~260 cm^{-1} in

z-Se for all the E directions. In addition, z-Se presents small humps at ~380 cm^{-1} and ~510 cm^{-1}, the intensities varying from sample-to-sample and with measuring conditions. The 380 cm^{-1} peak will be discussed later, while it is straightforward to identify the 510 cm^{-1} peak as an overtone of the 260 cm^{-1} [8].

Fig. 3 shows x-ray diffraction patterns obtained for assemblages of pure ZSM-5 and z-Se at scattering angle 2θ in the range of 5 to 35°. At higher angles up to 60°, there have been no discernible differences between the two profiles. We see in Fig. 3 that ZSM-5 shows Bragg peaks at $2\theta \approx$ 8-10°, 14°, and 23°, the pattern resembling that reported previously [16]. Z-Se produces a clear peak at ~27°, which indicates the existence of crystalline planes with a separation of ~0.33 nm. The peak width of ~0.5°, which may be still influenced by widths of diffractometer slits, suggests a crystal thickness of greater than ~80 nm through the Scherrer equation.
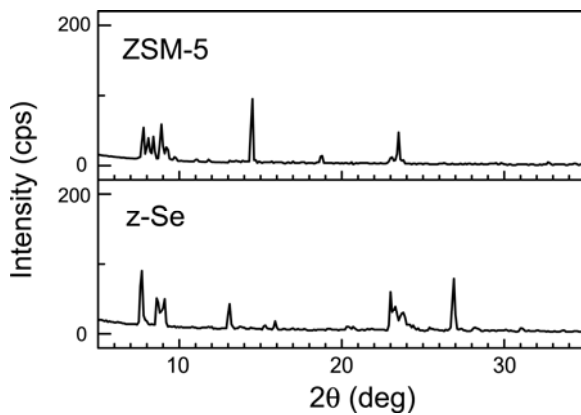

Fig. 3. Transmission x-ray diffraction patterns of ZSM-5 and z-Se on highly-oriented pyrolytic graphite substrates.

An assemblage (~1000 pieces) of z-Se has exhibited a strong and sharp ESR signal. As shown in Fig. 4(a), pure ZSM-5 and Se chunks have not presented any ESR signals. In contrast, z-Se exhibits a clear peak with the g-value and the half width of ~2.00 and ~1 mT, which scarcely changes with temperatures at 80 and 290 K (Figs. 4(b) and (c)). The integrated signal, suggesting a spin density of ~10^{13} /piece, also unchanges with temperature. It is known that pure Se bulk samples produce detectable ESR signals at $g \simeq 2.00$ only under light irradiation at low temperatures, while the peak is much broader ~20 mT [19, 20]. On the other hand, it has been demonstrated that oxidized Se samples exhibit a sharp signal, the shape being very similar to the present one, which is ascribed to oxygen charge-transfer complexes, which terminate Se chains [18, 21].

As shown in Fig. 4 (d), the ESR signal is photo-enhanced. Illumination of 2.0 eV light with an intensity of ~1 mW (~100 mW/cm^2) for a few minutes at room temperature has increased the signal keeping the spectral shape unchanged. The increase is by an order, suggesting ~10^{14} spin/piece, which scarcely changes upon prolonged illumination. Quantum efficiency of this photoinduced process, estimated from a ratio of the spin density (~10^{14} spin/piece) divided by the absorbed photon dose [22] (10^{15}-10^{16} /piece), is 10^{-2}-10^{-1}. The increased signal stays in stable after terminating the illumination, at least, for 3 days at room temperature. It is mentioned that exposures using a 2.3 eV laser and a Xe lamp have brought similar increases in the spin signal, which suggests that the saturated spin density does not depend critically on the photon energy of excitation.
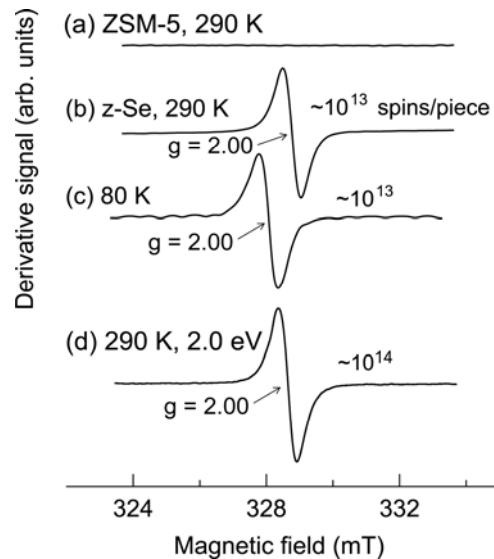

Fig. 4. ESR spectra of (a) ZSM-5 at room temperature, and z-Se at (b) 290 K and (c) 80 K, (d) 290 K after illumination of light with 2.0 eV, ~1mW, and ~5 min. The shift of the resonance field with temperature is instrumental.

It should be mentioned that the present ESR result is contrastive to those previously reported [5, 19, 20, 23]. For instance, a-Se does not give no dark ESR signals, and illumination of bandgap light at cryogenic temperatures induces broad signals (~20 mT) at $g \approx 2$ with spin densities of 10^{16} ~ 10^{19} cm^{-3}, which is ascribed to dangling bonds of Se [24].

Fig. 5 shows optical absorption (attenuation) spectra of z-Se and a-Se [18, 25, 26]. Z-Se exhibits substantial light scattering, and accordingly, the spectra have been evaluated in two ways. The solid line is calculated from the transmittance obtained using the conventional spectrometer. On the other hand, the circles connected by a dashed line are obtained from measurements using lasers and photo-detectors, which are located just after the sample, so that the spectrum is less influenced by light scattering. The two results seem to coincide above ~2.2 eV. Spectra outside of 1.7-2.4 eV could not be evaluated due to the fixed shapes of the present samples. An optical gap energy, which may be defined as a photon energy at an absorption coefficient of 10^3 cm^{-1}, is located at ~2.2 eV. It is blue-shifted by ~0.4 eV from that of ~1.8 eV [18, 26, 27] in a-Se at room temperature.
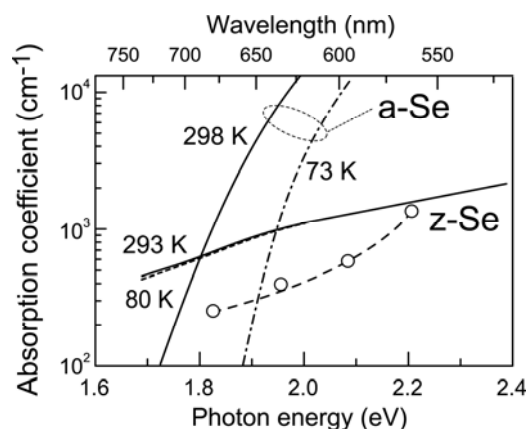
Fig. 5. Optical absorption spectra of z-Se and a-Se. The solid line and the circles for z-Se are obtained using a conventional spectrometer and the laser measurement (polarization unresolved). Results for a-Se at 73 and 298 K [26] are also shown for comparison.
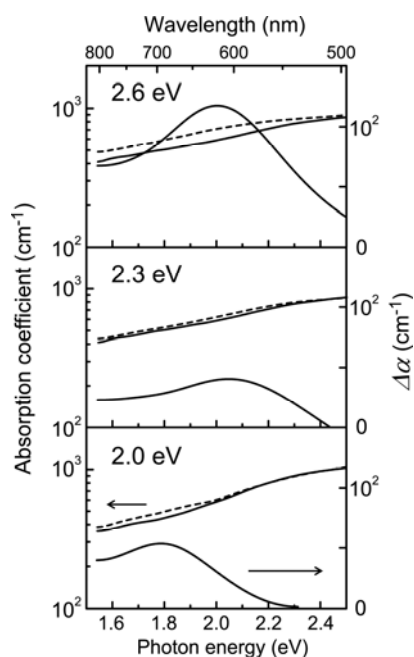

Fig. 6. Photoinduced absorption changes by laser lines (2.0-2.6 eV) in z-Se.

Fig. 6 shows that z-Se undergoes photoinduced absorption at 1.6-2.4 eV at room temperature. In detail, the induced absorption has a peak, which is located at ~1.8 eV under excitation of 2.0 eV and at ~2.0 eV under excitations of 2.3 and 2.6 eV. It should be noted that the growing timescale of the induced absorption is much longer than that of the photoinduced ESR. For instance, under the 2.0 eV excitation, the absorption saturation occurs after ~1 h, being longer by an order than that of the spin increase. This induced absorption is stable, at least, for ~10 h. It is mentioned that intense excitation of 2.8 eV has gradually bleached the sample and ultimately the sample becomes transparent, which may be due to sublimation of Se.
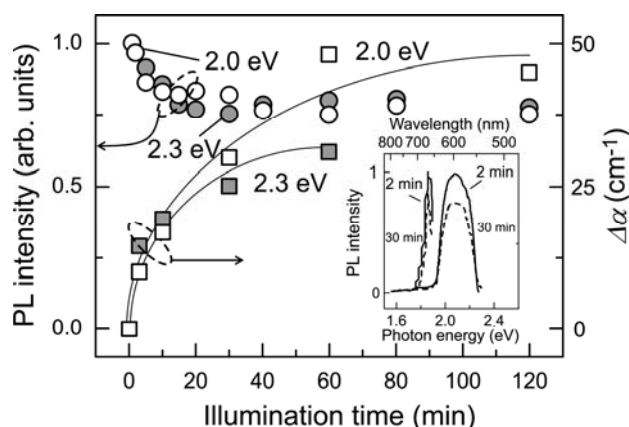

Fig. 7. PL fatigue (circles) and induced absorption (squares) by laser light of 2.0 eV and 1 mW (open symbols), and 2.3 eV and 40 mW (solid symbols). Curves are guided for eyes. Inset shows PL spectra after exposures of 2 min (minimal detection period, solid lines) and 30 min (dashed lines) with 2.0 eV (left peak) and 2.3 eV (broader right peak) light.

The PL fatigues upon light excitation at room temperature. For instance, as shown in Fig. 7, upon irradiation of the 2.0 eV light, PL weakens to ~70% with a timescale of ~1 h, which is similar to that of the induced absorption. The fatigue level is, for excitation of 2.0-2.5 eV, 50-70%, which seems to vary from sample-to-sample. However, in contrast to those in the ESR and absorption changes, the PL fatigue has recovered at room temperature with a timescale of ~10 h. Then, the PL again weakens under repeated excitation.

To the authors' knowledge, the present phenomena give the first observation of the photoinduced absorption and PL fatigue in Se. It should be also mentioned here that Raman-scattering spectroscopy could detect no structural modifications corresponding to the three photoinduced changes.

4. Discussion

Macroscopic observations have provided two insights. One is the inhomogeneous loading of Se, which is suggested from the spatial color variation of z-Se samples in Fig. 1. On the other hand, the weight loss measurement suggests that the pores in ZSM-5 are mostly occupied by Se atoms.

The Raman-scattering spectroscopy manifests that the short-range structure of Se clusters in ZSM-5 is not very different from those in t-Se and a-Se. That is, since all the substances exhibit the main peaks at 240-260 cm^{-1}, we envisage similar structures with the atomic coordination of 2, nearest neighbor distance of ~0.23 nm, and bond angle of ~105°[18, 29]. We then assume Se chains or rings. However, ring molecules such as Se_8, which is reported to give a peak at ~270 cm^{-1} [30], are appreciably greater in size (~0.9 nm) than the pore diameter in ZSM-5 [14-16],

and accordingly, the existence can be dismissed. For the chains, it is known that the position of the main Raman-scattering peak, arising from a symmetric bond stretching mode, shifts to higher wavenumbers with decreasing inter-molecular interaction; from 236 cm^{-1} in t-Se to ~260 cm^{-1} in isolated Se chains [18, 30]. This fact suggests that loaded Se in ZSM-5, showing the slightly higher peak position (~260 cm^{-1}) than those of t-Se and a-Se, takes chain forms with little inter-chain interaction, which possibly suggests the existence of single Se chains. On the other hand, the 380 cm^{-1} peak is assigned to a Se dimer, which is known to be stable in Se vapors [9, 31-34]. We therefore conclude that Se in ZSM-5 takes chain structures, having negligible inter-chain interaction, and dimers.

The chain length can be estimated. The weight-loss measurement has suggested a Se density of ~10^{15} atom/piece, and the ESR signal, which is attributable to the oxygen charge-transfer complex, presents a spin density of ~10^{13} /piece [18, 21]. Accordingly, we envisage a single chain of ~10^2 Se atoms, the ends being terminated by O$_2$ molecules. It is not known, however, whether the chain length distributes at 2-10^2 or 2 and ~10^2.

The result for x-ray diffraction patterns is difficult for interpretation. The distance is clearly longer than the first nearest-neighbor distance of 0.23 nm in Se solids and slightly shorter than the second nearest-neighbor distance of 0.37 nm [18]. Otherwise, we notice that this separation is similar to that (0.33 nm) of crystalline 101 faces in t-Se [29]. But, it is doubtless that t-Se cannot geometrically exist in such narrow pores in ZSM-5. In addition, the existence of t-Se is also in conflict with the Raman peak position, as discussed above, and with the blue-shifted and temperature-independent optical absorption edge (Fig. 5).
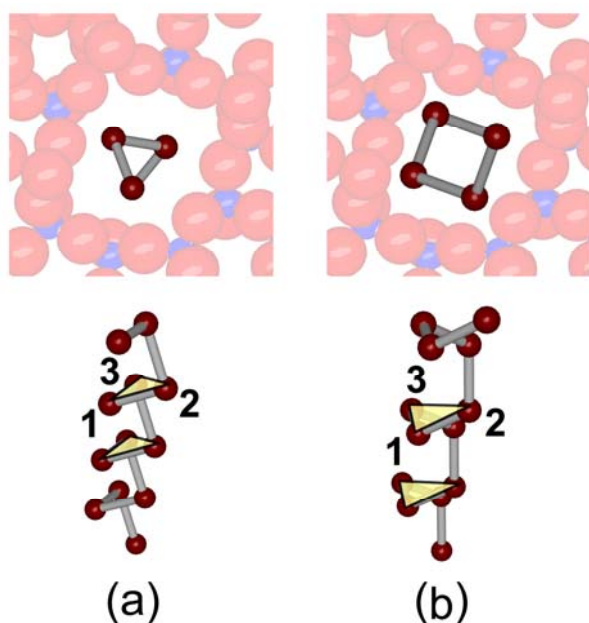

Fig. 8. Cross-sectional (upper) and three-dimensional (lower) views of single (a) 3-fold, (b) 4-fold helical chains in ZSM-5 pores.

Table.1. Comparison of 3- [29] and 4-fold helices having a bond length of 0.23 nm and a bond angle of 105°.

Helix	Rotating angle	Helix diameter (framework)	Helix pitch	Plane separation
3-fold	120°	0.19 nm	0.50 nm	0.22 nm
4-fold	90°	0.28	0.74	0.37

It may be straightforward to consider a single 3-fold helical chain (Fig. 8(a)), which exists in t-Se. The chain has a framework helix diameter of 0.19 nm (Table I) [35], so that the van-der-Waal diameter is estimated at ~0.6 nm [36], which can geometrically exist in the zeolite pore (a framework diameter of ~0.83 nm and free diameter of ~0.56 nm). In the 3-fold chain, trimers -Se-Se-Se- fix small and parallel planes, the one being indicated as 1-3 in Fig. 8(a). A series of the parallel planes may give Bragg peaks. However, the plane separation is calculated to be ~0.22 nm, substantially shorter than the experimentally obtained distance of ~0.33 nm. Accordingly, we neglect this structure.

Next, we propose a single 4-fold helix, illustrated in Fig. 8(b). In such modified structures, however, the bond length (~0.23 nm) and bond angle (~105°) can possibly be retained due to big strain energies. A simple analysis under this condition shows that the 4-fold helix has framework and van-der-Waals diameters of 0.28 nm and ~0.68 nm (Table I), which are appreciably smaller than or comparable to the pore diameters of ZSM-5. In addition, the separation between the trimer plane (1-3 in Fig. 8(b)) is ~0.37 nm, nearly the same with $d \approx 0.33$ nm. That is, this model is able to explain the position of the diffraction peak. A remaining problem is that single chains with small crystalline planes can give such a narrow diffraction peak as the width of ~0.5°. A single chain of ~10^2 atoms has a typical length of ~20 nm, while it is not evident if the fragmental plane can give the sharp peak. Otherwise, we may speculate that several chains aligning in parallel pores in ZSM-5 (see, Fig. 1) cooperatively diffract the incident x-ray beam, producing the sharp peak.

The blue-shifted absorption edge (Fig. 5) can be ascribed to the single chain structure. Theoretical calculations [37-40] demonstrate that the inter-chain interaction makes the energy width of the valence band, arising from the lone-pair electron state, broader by 1-2 eV. Accordingly, we expect that the single chain has a greater HOMO-LUMO gap by ~1 eV than the bandgap in t-Se. The gap is near to the observed blue-shift of ~0.4 eV. Otherwise, the shift can be understood as a one-dimensional quantum-well effect, which is estimated from $\Delta E = (\pi^2 \hbar^2/2m) \Sigma_i (1/L_i^2)$, where m is a carrier mass and L_i a well side-length (or an electronic mean-free path if it is shorter). Provided that m to be the free-electron mass and a rectangular well with a length of 1-20 nm and side lengths of 0.7 nm (van-der-Waals helix diameter), we also obtain $\Delta E \approx 0.1$-1.0 eV. The very small temperature dependence of the absorption edge may imply weak

electron-vibration coupling arising from non-existence of inter-chain interaction [27], which is consistent with the single chain structure.

The problem is if the photoinduced changes in ESR, optical absorption, and PL for z-Se at room temperature arise from a unique structural change. The related timescales of photo-inductions and thermal recoveries are different. As mentioned, upon illumination of 2.0 eV light of ~100 mW/cm^2, the spin increase, induced optical absorption, and PL fatigue have occurred, respectively, with the timescales of ~ 5 min, ~ 1 h, and ~ 1h. And, only the PL fatigue has recovered after storage in the dark at room temperature for ~10 h. (2.3 eV light has given similar features, while those may be affected by light-penetration effects.). Therefore, we should consider the origins of these photoinduced changes one-by-one, taking the suggested Se structure into account.

Mechanism of the photo-enhanced ESR relies upon an interpretation of the dark signal because of the very similar shapes. Abkowitz and others have ascribed the sharp ESR signal in solid Se to the oxygen charge-transfer complex [18, 21], which may be denoted as $Se^+ O_2$, where Se symbolizes a chain end. This interpretation provides a model for the photoinduced ESR in z-Se that light illumination cuts single Se chains, a kind of chain fragmentation process, and the broken ends immediately form the oxygen complexes as $Se^+ O_2 O_2 Se^+$. It seems that O_2 exists anywhere, since it can easily penetrate into the pore due to the small elliptical shape of ~0.3 nm and ~0.4 nm. Otherwise, O_2 may be supplied from the inner walls of ZSM-5 pores. Taking the Se density of $\sim10^{15}$ /piece and the photoenhanced spin density of $\sim10^{14}$ /piece, we now assume that the chain length is reduced to ~10 atoms on average. It is known that, in solid and molecular Se, the valence band and HOMO level are made from lone-pair electron states, not from bonding states [37, 41, 42]. Hence, if excitation of a lone-pair electron can cut a covalent bond has not been clear. But, the photoinduced ESR evinces the scission, in consistent with a molecular-dynamics simulation for an infinitely-long Se chain at 500 K [43], which demonstrates photoinduced states-hybridization leading to bond breaking. It is plausible that such bond scission assists the photoinduced crystallization [44-46].

For the induced absorption, the origin is not clear understood. The spectral shape suggests that the induced absorption is not the photodarkening [47-49], which denotes a nearly-parallel red-shift of the absorption edge [24, 44, 50]. The photodarkening is believed to arise from enhanced disordering in inter-chain interaction [24], and accordingly, its non-existence in single Se chains is reasonable. On the other hand, it cannot be known if the induced absorption can be regarded as the mid-gap absorption extending at $E_g/2 \sim E_g$ (E_g is the optical gap) [24], since the lower energy side ($\sim E_g/2$) could not be inspected due to the limited size of z-Se samples. Since the induced absorption shows a longer growing timescale than that of the ESR, we should assume some ESR-inactive structural changes which occur in the shortened Se chains.

For an interpretation of the PL fatigue at room temperature, the origin of the PL should be known. Here, we underline the small Stokes shift of 0.1-0.2 eV, which implies that the PL arises from exciton (electron-hole pair) recombination. Since the exciton is produced in the deformable single chains, polaronic excitons may be responsible for the PL. This view seems to be consistent with a theoretical result by Ikawa and Fukutome [37] and previous experimental results for t-Se [51] and for Se in another kind of zeolite 13X [8]. It seems that Se in ZSM-5 works as a dye in a wide-gap host. It should be noted that the small Stokes shift in z-Se is contrastive to those reported for a-Se [52], t-Se [53], and Se-cancrinite [10], in which the PL peak-energy E_{PL} satisfies the so-called half-gap rule, $E_{PL} \simeq E_g/2$, which is widely observed in chalcogenide glasses and corresponding crystals [52], although the origin remaining controversial [24, 54].

We can interpret the PL fatigue in z-Se below. Since it occurs with a similar timescale to the induced absorption, while it thermally recovers at room temperature, we may envisage additional changes to that causing the induced absorption. For instance, ESR inactive bi-excitons are self-trapped at the distorted segment or the oxidized sites as $Se^+ O_2 O_2 Se^+$. Provided that such excitons have a life time of ~10 h, the PL may fatigue due to a limited density of the trapping sites.

5. Conclusions

We have studied the atomic structure, optical properties, and photoinduced effects of Se in a covalent zeolite, sub-mm size ZSM-5 single crystals, and obtained the following conclusions:

(1) Loaded Se atoms appear to form single 4-fold helical chains with atomic lengths of $\sim10^2$ and dimers. The optical absorption edge blue-shifts from those in a-Se by ~0.4 eV, which can be connected with the single chain structure.

(2) Se-loaded ZSM-5 exhibits, at room temperature, photoinduced phenomena including photoinduced ESR, sub-gap absorption, and PL fatigue. The photoinduced ESR arises from the bond scission in single Se chains. The sub-gap absorption and PL fatigue occur with a longer timescales than that of ESR, and only the PL shows a recovery. PL possibly arises from self-trapped (polaronic) excitons in single Se chains, and the fatigue can be related to a finite exciton lifetime.

References

[1] H. S. Nalwa, Handbook of Advanced Electronic and Photonic Materials and Devices, in, Academic Press, San Diego, **6**, 2001.

[2] S. A. Averkiev, L. S. Agroskin, V. G. Aleksandrov, V. N. Bogomolov, Y. N. Volgin, A. I. Gutman, T. B. Zhukova, V. P. Petranovskiî, D. S. Poloskin, L. P. Rautian, S. V. Kholodkevich, Sov. Phys. Solid State **20**, 251 (1978).

[3] V. N. Bogomolov, V. V. Poborchii, S. V. Kholodkevich, S. I. Shagin, JETP Lett. **38**, 532 (1983).

[4] V. N. Bogomolov, S. V. Kholodkevich, S. G. Romanov, L. S. Agroskin, Solid State Commun. **47**, 181 (1983).

[5] Y. Katayama, M. Yao, Y. Ajiro, M. Inui, H. Endo, J. Phys. Soc. Jpn. **58**, 1811 (1989).

[6] Y. Nozue, T. Kodaira, O. Terasaki, K. Yamazaki, T. Goto, D. Watanabe, J. M. Thomas, J. Phys. Condens. Mat. **2**, 5209 (1990).

[7] K. Matsuishi, T. Isome, J. Ohmori, S. Onari, T. Arai, Phys. Stat. Sol. (b) **215**, 301 (1999).

[8] L. He, Z. X. Shen, G. Gu, L. Qin, S. H. Tang, Chem. Phys. Lett. **300**, 504 (1999).

[9] A. V. Kolobov, H. Oyanagi, V. V. Poborchii, K. Tanaka, Phys. Rev. B **59**, 9035 (1999).

[10] V. V. Poborchii, G. G. Lindner, M. Sato, J. Chem. Phys. **116**, 2609 (2002).

[11] P. Simoncic, T. Armbruster, Microporous and Mesoporous Materials **71**, 185 (2004).

[12] A. Goldbach, L. E. Iton, M. Grimsditch, M. L. Saboungi, Chem. Mat. **16**, 5107 (2004).

[13] I. L. Li, S. C. Ruan, Z. M. Li, J. P. Zhai, Z. K. Tang, Appl. Phys. Lett. **87**, 071902 (2005).

[14] G. T. Kokotailo, S. L. Lawton, D. H. Olson, W. M. Meier, Nature **272**, 437 (1978).

[15] H. V. Koningsveld, J. C. Jansen, H. V. Bekkum, Zeolites **10**, 235 (1990).

[16] S. Shimizu, H. Hamada, Microporous and Mesoporous Mat. **48**, 39 (2001).

[17] A. Saitoh, K. Tanaka, Solid State Commun. **149**, 750 (2009).

[18] R. A. Zingaro, W. C. Cooper, Selenium, in, Van Nostrand Reinhold, New York, 1974.

[19] S. G. Bishop, U. Strom, P. C. Taylor, Phys. Rev. Lett. **36**, 543 (1976).

[20] A. V. Kolobov, M. Kondo, H. Oyanagi, A. Matsuda, K. Tanaka, Phys. Rev. B **58**, 12004 (1998).

[21] M. Abkowitz, J. Chem. Phys. **46**, 4537 (1967).

[22] A. Saitoh, K. Tanaka, J. Appl. Phys. **105**, 113531 (2009).

[23] L. N. Blinov, Glass Phys. and Chem. **29**, 203 (2003).

[24] K. Shimakawa, A. Kolobov, S. R. Elliott, Adv. Phys. **44**, 475 (1995).

[25] K. J. Siemens, E. W. Fenton, Phys. Rev. Lett. **161**, 632 (1967).

[26] J. Stuke, J. Non-cryst. Solids **4**, 1 (1970).

[27] G. G. Roberts, S. Tutihasi, R.C. Keezer, Phys. Rev. Lett. **166,** 637 (1968).

[28] W. Henrion, Phys. Stat. Sol. **7**, 189 (1964).

[29] P. Andonov, J. Non-cryst. Solids **47**, 297 (1982).

[30] V. V. Poborchii, A. V. Kolobov, H. Oyanagi, S. G. Romanov, K. Tanaka, Chem. Phys. Lett. **280**, 10 (1997).

[31] A. Goldbach, L. Iton, M. Grimsditch, M. L. Saboungi, J. Am. Chem. Soc. **118**, 2004 (1996).

[32] A. Goldbach, M. Grimsditch, L. Iton, M. L. Saboungi, J. Phys. Chem. B **101**, 330 (1997).

[33] V. V. Poborchii, J. Phys. Chem. Solids **55**, 737 (1994).

[34] S. Kohara, A. Goldbach, N. Koura, M. L. Saboungi, L. A. Curtiss, Chem. Phys. Lett. **287**, 282 (1998).

[35] R. M. Martin, G. Lucovsky, Phys. Rev. B **13**, 1383 (1976).

[36] L. Pauling, The nature of the chemical bond and the structure of molecules and crystals: an introduction to modern structural chemistry, Cornell University Press, New York, 1960.

[37] A. Ikawa, H. Fukutome, J. Phys. Soc. Jpn. **59**, 1002 (1990).

[38] I. Chen, Phys. Rev. B **7**, 3672 (1973).

[39] J. D. Joannopoulos, M. Shluter, M. L. Cohen, Phys. Rev. B **11**, 2186 (1975).

[40] T. Yamaguchi, F. Yonezawa, J. Non-cryst. Solids **156-158**, 268 (1993).

[41] A. A. Demkov, O. F. Sankey, J. Phys.: Condens. Mat. **13**, 10433 (2001).

[42] M. Kastner, Phys. Rev. Lett. **28**, 355 (1972).

[43] K. Hoshino, F. Shimojo, T. Nishida, J. Phys. Soc. Jpn. **68**, 1907 (1999).

[44] M. A. Popescu, Non-Crystalline Chalcogenides, in, Kluwer Academic Publishers, Dordrecht, 2000.

[45] J. Dresner, G. B. Stringfellow, J. Phys. Chem. Solids **29**, 303 (1968).

[46] K. Ishida, K. Tanaka, Phys. Rev. B **56**, 206 (1997).

[47] K. Tanaka, A. Odajima, Solid State Commun. **43**, 961 (1982).

[48] A. Reznik, B. J. M. Lui, J. A. Rowlands, S. D. Baranovskii, O. Rubel, V. Lyubin, M. Klebanov, S. O. Kasap, J. Appl. Phys. **100**, 113506 (2006).

[49] A. Reznik, M. Klebanov, V. Lyubin, J. Appl. Phys. **105**, 013518 (2009).

[50] A. V. Kolobov, Photo-Induced Metastability in Amorphous Semiconductors, in: A.V. Kolobov (Ed.), Wiley-VCH, Winheim, 2003.

[51] S. Tutihasi, I. Chen, Phys. Rev. **158**, 623 (1967).

[52] R. A. Street, Adv. Phys. **25**, 397 (1976).

[53] H. Lundt, G. Weiser, Solid State Commun. **48**, 827 (1983).

[54] J. Ristein, P. C. Taylor, W. D. Ohlsen, G. Weiser, Phys. Rev. B 42, **11845** (1990).

_____

[*]Corresponding author: asaito@ehime-u.ac.jp